Understanding the Effect of Synthesis and Sintering Temperature on the Functional Properties of Barium Titanate/Cobalt Ferrite Composites

Marija Šuljagić[1], Aleksandar Kremenović[2], Ivan Petronijević[3], Adis Džunuzović[4], Miljana Mirković[5], Vladimir Pavlović[6], Ljubica Andjelković[1*)]

[1]University of Belgrade-Institute of Chemistry, Technology and Metallurgy, Department of Chemistry, Njegoševa 12, Belgrade, Serbia
[2]Faculty of Mining and Geology, University of Belgrade, Djušina 7, 11000 Belgrade, Serbia
[3]Faculty of Physics, University of Belgrade, Studentski Trg 12-16, Belgrade, Serbia
[4]Institute for Multidisciplinary Research, University of Belgrade, Volgina 15, Belgrade, Serbia
[5]Department of Materials „Vinča" Institute of Nuclear Sciences - National Institute of the Republic of Serbia, University of Belgrade, Belgrade, Serbia
[6]University of Belgrade, Faculty of Agriculture, Nemanjina 6, Zemun, Belgrade, Serbia

Abstract:
    To investigate the effect of synthesis procedure and sintering temperature on the functional properties of perovskite/spinel ceramics, $BaTiO_3/CoFe_2O_4$ composites were prepared by thermal decomposition, coprecipitation, and microemulsion method, and sintered at 1150°C and 1300°C. The phase composition and morphology of as-prepared powders as well as sintered ceramics were thoroughly examined by X-ray powder diffraction (XRPD) and scanning electron microscopy (SEM) coupled with electron dispersive spectroscopy (EDS). The dielectric and ferroelectric measurements were performed in detail. Generally, the samples sintered at 1300°C had better performances than those sintered at 1150°C. The composite synthesized by thermal decomposition and sintered at 1300 °C stands out among other prepared $BaTiO_3/CoFe_2O_4$ ceramics, owing to high stability in the wide frequency range and low leakage currents. The obtained results indicate that such composite might be successfully applied as a functional multiferroic.
Keywords: *Perovskite/spinel ceramics; Multiferroic; Sintering; Influence of synthesis method.*

1. Introduction

    The possibility to combine spinel ferrites and perovskites allowing outstanding performances and multifunctionality *via* coupling between ferromagnetic and ferroelectric phase have attracted an immense scientific interest [1–7]. Barium titanate ($BaTiO_3$) with

_____

) **Corresponding author: ljubica@chem.bg.ac.rs*

perovskite structure possesses promising electric properties [8–10] which enable its wide usage in the field of electronic industry, as a part of multilayer ceramic capacitors [11], piezoelectric transducers [12], electro-optic devices [13] and thermistors [14]. On the other hand, spinel ferrites are well-known magnetic materials [15–17] which can be used in drug delivery systems [18,19], microwave devices [20,21], data storage [22], catalysis [23] etc. Cobalt ferrite ($CoFe_2O_4$) stands out among other spinel oxides due to the highest magnetostriction coefficient, highly desirable property in magnetoelectric composites. Hence, such composites containing $BaTiO_3$ and $CoFe_2O_4$, are of great scientific and technological interest. They could be successfully applied in technology as microwave devices, antennae, sensors, transducers, data storage [24–29]. The potential use of such systems for controlled release of anti- HIV drug delivery and neurostimulation to treat Alzheimer's and Parkinson's disease should not be overlooked [30–35].

The key factors to achieve good magnetoelectric response are phase composition and amount, particle size, and porosity which could be controlled by performed synthetic route and chosen sintering temperature. The main disadvantages of conventionally used mixture method are the large particle size, high porosity, poor dispersion of components, interphase reactions and atomic interdiffusion [36]. Since mentioned factors deteriorate electric and magnetic properties, the efforts should be put in their prevention. The increase in spinel phase content negatively influence magnetoelectric response owing to leakage currents caused by the low resistivity of the high conductive ferrite phase [37]. Higher sintering temperature leads to better mechanical coupling between the ferrite and ferroelectric grains, necessary for high magnetoelectric signal. On the other hand, such high temperatures may induce formation of Fe^{2+} ions in ferrites causing interphase reactions. The occurrence of divalent Fe ions decreases electric resistivity, and thus lowers magnetoelectric signal [37]. Special attention should be also paid to the synthesis of $BaTiO_3$ in appropriate crystal form, since only tetragonal $BaTiO_3$ with *P4mm* space group possesses piezoelectric properties due to the absence of inversion centre.

The aim of this study was to investigate influence of synthesis procedure as well as sintering temperature on $BaTiO_3/CoFe_2O_4$ functional properties. The samples were synthesized by thermal decomposition, coprecipitation, and microemulsion method, and sintered at 1150 and 1300°C. Detailed impedance spectroscopy and ferroelectric measurements were performed.

2. Materials and Experimental Procedures
2.1 Synthesis

In all cases $CoFe_2O_4$ nanoparticles were *in situ* synthesized on commercial $BaTiO_3$. All chemicals (barium titanate ($BaTiO_3$, 99%), acetylacetone, ammonium hydroxide solution (28% NH_3 in water), iron (III) chloride hexahydrate ($FeCl_3·6H_2O$, 98%), cobalt (II) chloride hexahydrate ($CoCl_2·6H_2O$, 98%), sodium hydroxide (NaOH,>97%), cetyltrimethylammonium bromide (CTAB,>98%), n-butanol (99.8%), n-hexanol (>99%), and absolute ethanol) were obtained from Sigma-Aldrich.

2.1.1 BaTiO₃/CoFe₂O₄ thermal decomposition synthesis

The iron(III) acetylacetonate and cobalt(II) acetylacetonate complexes were used as the precursors for the synthesis of $CoFe_2O_4$ nanoparticles. These precursors were synthesized in a reaction of appropriate metal ions (Fe^{3+} or Co^{2+}) with ammonium acetylacetonate. Ammonium acetylacetonate was prepared using deprotonation reaction of acetylacetone by the ammonia solution. The obtained acetyacetonates (0.026 mol of $Fe(acac)_3$ and 0.013 mol of

_____

$Co(acac)_2$) were pulverized in the agate mortar with 0.013 mol of $BaTiO_3$. The appropriate amount of toluene was added, and the mixture of paste-like consistency was formed. The combustion reaction started using a Bunsen burner. After pulverization process, the partly decomposed mixture was heated in an electric furnace at 500°C for 1 h. The final product was also pulverized in agate mortar.

2.1.2 $BaTiO_3$/$CoFe_2O_4$ coprecipitation synthesis

Cobalt ferrite was synthesized from chloride salts of Co(II) and Fe(III). Barium titanate (0.013 mol) was suspended in water solution (300 mL) that contained $FeCl_3 \cdot 6H_2O$ (0.026 mol) and $CoCl_2 \cdot 6H_2O$ (0.013 mol). The mixture was heated until boiling point was reached and then excess of NaOH solution was added (<1.04 M, 100 mL). The pH value of suspension was above 9. The obtained suspension has been heated for 1 h. After cooling at room temperature, the precipitate was collected and rinsed with deionized water three times to remove the excess of residual ions. The dried product was pulverized in an agate mortar and annealed in an electrical furnace at 500°C for 1 h.

2.1.3 $BaTiO_3$/$CoFe_2O_4$ microemulsion synthesis

CTAB as the surfactant, n-butanol as the co-surfactant, n-hexanol as the oil phase and an aqueous solution as the water phase were used to obtain the microemulsion system. The microemulsion was composed of 15 wt% hexanol and 45 wt% aqueous solution. CTAB to n-butanol ratio was 60:40. Two microemulsions with different aqueous phases were prepared. The first microemulsion comprise of $FeCl_3 \cdot 6H_2O$ (0.026 mol), $CoCl_2 \cdot 6H_2O$ (0.013 mol), and $BaTiO_3$ (0.013 mol) suspension, while the second microemulsion water phase contained an aqueous solution of ammonia (<0.104 mol). The obtained microemulsions have been heated for 1h at 90°C. After precipitation occurred, the pH value was about 10. Then, water/ethanol mixture was added to the final microemulsion, and precipitated by centrifugation. In order to remove residues of oil and surfactant, the precipitate was washed with absolute ethanol several times, then with water/ethanol mixture (50:50) and, separated from the solution by vacuum filtration. After drying at room temperature, the precipitate was pulverized in the agate mortar and annealed in the electrical furnace at 500 °C for 1 h.

2.1.4. Sintering

After the initial preparation procedures, the synthesized powders were compressed into the pellets at 300 MPa using a uniaxial double action pressing process with an 8mm diameter tool, hydraulic press RING, P-14, VEB THURINGER. The pellets were sintered at two temperatures, 1150 and 1300°C, in electrical tube furnace (up to 1500°C) equipped with LAND calibration source. Heating rate was 15 °C/min to 1000°C and 5 °C/min until chosen temperatures were reached. The samples have been sintered at both temperatures for 2.5 h and removed from furnace after spontaneously cooling to room temperature.

2.2 Characterization

X-ray powder diffraction (XRPD) was used to characterize the synthesized samples at room temperature by Ultima IV Rigaku diffractometer, equipped with $CuK_{\alpha1,2}$ radiation, using a generator voltage (40.0 kV) and a generator current (40.0 mA). The continuous scan mode with a scanning step size of 0.02° and at a scan rate of 5°/min was used in the range between 10° and 80° 2θ, using D/TeX Ultra high - speed detector. Samples were prepared on Si-monocrystalline sample carrier. Phase composition of synthesized composites as well as

_____

phase abundances are calculated by RIR method incorporated in PDXL2 integrated X-ray powder diffraction software (Version 2.8.30; Rigaku Corporation).

To get deeper insight into the morphology and composition of prepared materials scanning electron microscopy (SEM) performed on JEOL JSM-6390 LV coupled with electron dispersive spectroscopy (Oxford Instruments X-MaxN). As a standard part of the preparation process, samples placed on a carbon tape were covered with gold to achieve conductive coating. The accelerating voltage in the SEM was in the range 20-30 kV.

Dielectric properties of the samples were obtained by measurements with two digital LCR meters: Hameg 8118 (from 20 Hz to 90 kHz) and Agilent 4285A (from 90 kHz to 9 MHz). Frequency spectrums were merged to obtain broader frequency dependence of dielectric parameters (tg δ, ϵ`, $Z$`, Z``). Measurements were conducted under normal atmospheric pressure, ambient temperature, and relative humidity of 40%. The applied voltage across the closed micrometer capacitor cell was 1.5 V. The capacitor cell was housed in a Faraday cage.

For temperature dependence measurements samples was placed in vacuum chamber with cold head and capacitor cell mounted on it. Pfeiffer vacuum turbo molecular pump maintained 10^{-4} mbar pressure. CTI Cryogenics refrigerating system model 22 mounted on cold head was used to lower temperature at 150 K. Lakeshore 340 temperature controller with hater attached at cold head was used to gradual heating rate of 2.5 K/min up to 400 K.

Ferroelectric and leakage current measurements were performed in the electrical field range from 5 to 40 kV/cm on the Precision Multiferroic Test System with High Voltage Interface (Radiant Technologies, Inc.).

3. Results and Discussion

The X-ray powder diffractograms for $BaTiO_3/CoFe_2O_4$ composites are presented in Fig. 1. The higher the temperature is, the better phase crystallinity occurred. The peaks in XRPD patterns got sharper due to the increased crystallinity of the samples. Change in sintering temperature from 1150°C to 1300°C led to more pronounced intensity of the reaction between $BaTiO_3$ and $CoFe_2O_4$. The detailed phase composition for as-prepared and sintered $BaTiO_3/CoFe_2O_4$ samples is shown in Table I. In the case of as-prepared powders, the pure spinel and tetragonal $BaTiO_3$ phases were obtained, irrespective of the performed synthesis procedure. After sintering, the barioferrite-like phases appeared. For sample synthesized by thermal decomposition, formation of CoO phase was observed at 1300°C. In all cases $BaTiO_3$ changed space group from *P4mm* to *P4/mmm* at 1300°C.

Tab. I Phase composition of synthesized composites. In parenthesis next to the phase chemical formulae crystal system and space group are presented as well as corresponding PDF card numbers from ICDD database. Phase abundances are calculated by RIR method.

Samples	Phase content		
$BaTiO_3/CoFe_2O_4$ thermal decomposition	$BaTiO_3$ Tetragonal (*P4mm*) PDF # 01-083-8300 63(2) %	$(Co_{0.255}Fe_{0.745})(Co_{0.745}Fe_{1.255})O_4$ Spinel (*Fd-3m*) PDF # 01-074-3419 37(2) %	/
$BaTiO_3/CoFe_2O_4$ coprecipitation	$BaTiO_3$ Tetragonal (*P4mm*) PDF # 01-083-8300 60(1) %	$(Co_{0.465}Fe_{0.535})(Co_{1.535}Fe_{0.465})O_4$ Spinel (*Fd-3m*) PDF # 01-074-3417 40(1) %	/

_____

BaTiO$_3$/CoFe$_2$O$_4$ microemulsion	BaTiO$_3$ Tetragonal (*P4mm*) PDF # 01-083-8300 49(2) %	(Co$_{0.15}$Fe$_{0.85}$)(Co$_{0.85}$Fe$_{1.15}$)O$_4$ Spinel (*Fd-3m*) PDF # 01-076-7254 51(2) %	/
BaTiO$_3$/CoFe$_2$O$_4$ thermal decomposition 1150 °C	BaTiO$_3$ Tetragonal (*P4mm*) PDF # 01-083-8300 61(1) %	(Co$_{0.15}$Fe$_{0.85}$)(Co$_{0.85}$Fe$_{1.15}$)O$_4$ Spinel (*Fd-3m*) PDF # 01-076-7254 15(1) %	BaFe$_{10.3}$Co$_{0.85}$Ti$_{0.85}$O$_{19}$ (*P6$_3$/mmc*) PDF # 01-073-7746 24(1) %
BaTiO$_3$/CoFe$_2$O$_4$ coprecipitation 1150 °C	BaTiO$_3$ Tetragonal (*P4mm*) PDF # 00-005-0626 7(1) %	CoFe$_2$O$_4$ Spinel (*Fd-3m*) PDF # 00-022-1086 23(2) %	Ba$_{12}$Fe$_{29.98}$Ti$_{13.72}$O$_{84}$ (*C2/m*) PDF # 01-085-2407 69(2) %
BaTiO$_3$/CoFe$_2$O$_4$ microemulsion 1150 °C	BaTiO$_3$ Tetragonal (*P4mm*) PDF # 01-083-830053(1) %	(Co$_{0.255}$Fe$_{0,745}$)(Co$_{0.745}$Fe$_{1.255}$)O$_4$ Spinel (*Fd-3m*) PDF # 01-074-3419 41(1) %	BaFe$_{10.3}$Co$_{0.85}$Ti$_{0.85}$O$_{19}$ (*P6$_3$/mmc*) PDF # 01-073-7746 6(1) %
BaTiO$_3$/CoFe$_2$O$_4$ thermal decomposition 1300 °C	BaTiO$_3$ Tetragonal (*P4/mmm*) PDF # 01-079-2264 49(1) %	(Co$_{0.255}$Fe$_{0,745}$)(Co$_{0.745}$Fe$_{1.255}$)O$_4$ Spinel (Fd-3m) PDF # 01-074-3419 3.1(2) % CoO (*Fm-3m*) PDF # 01-071-1178 2.7(2) %	BaFe$_{10.3}$Co$_{0.85}$Ti$_{0.85}$O$_{19}$ (P6$_3$/mmc) PDF # 01-073-7746 24(1) % Ba$_{13.97}$Fe$_{7.65}$Ti$_{15}$O$_{58.03}$ (*R-3m*) PDF # 01-072-5912 21(1) %
BaTiO$_3$/CoFe$_2$O$_4$ coprecipitation 1300 °C	BaTiO$_3$ Tetragonal (*P4/mmm*) PDF # 01-075-2121 21(1) %	CoFe$_2$O$_4$ Spinel (*Fd-3m*) PDF # 01-022-1086 70(2) %	BaFe$_{10.3}$Co$_{0.85}$Ti$_{0.85}$O$_{19}$ (*P6$_3$/mmc*) PDF # 01-073-7746 9(3) %
BaTiO$_3$/CoFe$_2$O$_4$ microemulsion 1300 °C	BaTiO$_3$ Tetragonal (*P4/mmm*) PDF # 01-079-2264 18(1) %	CoFe$_2$O$_4$ Spinel (*Fd-3m*) PDF # 00-022-1086 56(1) %	BaFe$_{10.3}$Co$_{0.85}$Ti$_{0.85}$O$_{19}$ (*P6$_3$/mmc*) PDF # 01-073-7746 26(1) %

According to SEM micrographs for as-prepared powders, the particles non-uniform in size and shape were observed, Fig. 2. The bigger particles between 600 and 1000 nm belonged to commercial BaTiO$_3$ while smaller ones in sub-100 nm range can be attributed to *in situ* synthesized CoFe$_2$O$_4$. The ferrimagnetic behaviour for ferrite particles was responsible for the pronounced agglomeration. The EDS layered images showed the best ferrite distribution over the titanate surface in the case of composite where CoFe$_2$O$_4$ was prepared by thermal decomposition method, Fig. 2. For the composites obtained by coprecipitation and microemulsion method, the regions where ferrite particles were localized, were observed, Fig. 2.
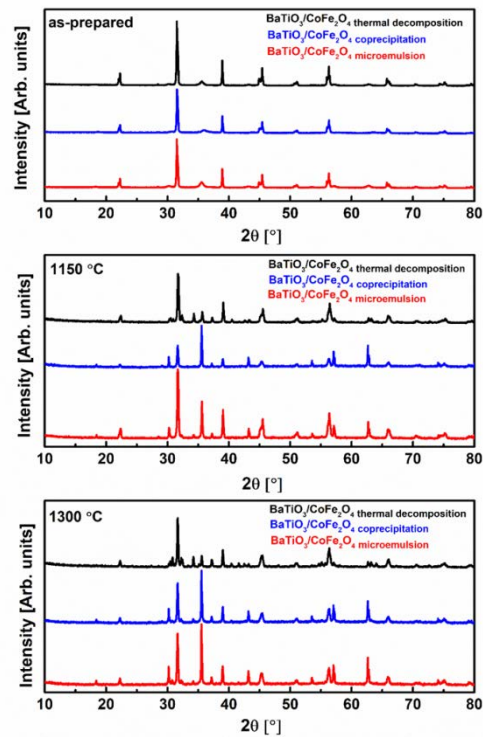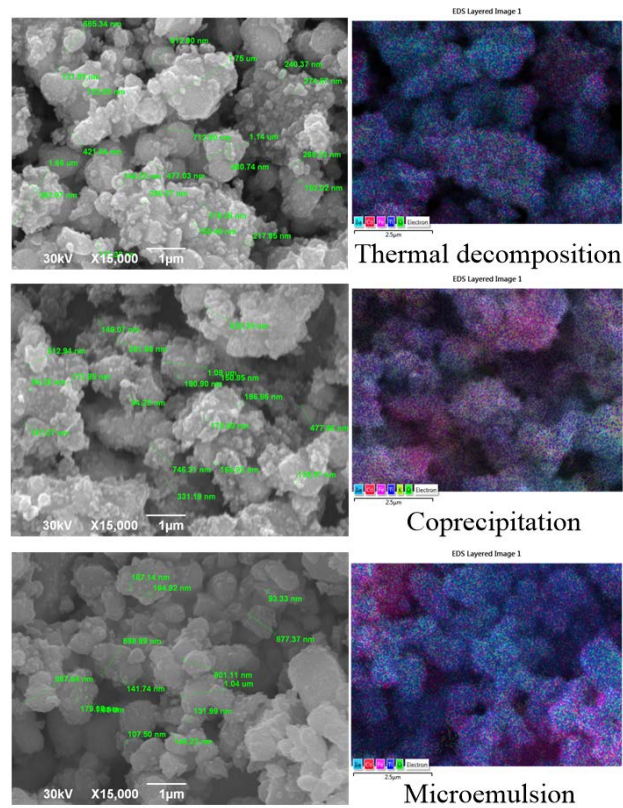
_____

Fig. 1. XRPD of BaTiO$_3$/CoFe$_2$O$_4$ samples.

Fig. 2. SEM and EDS layered images of non-sintered BaTiO$_3$/CoFe$_2$O$_4$ samples.

SEM micrographs of materials sintered at 1150°C indicated that sintering process was not completed at chosen temperature, Fig. 3. The presence of porosity and many particles which preserved their shape confirmed that only intermediate stage of sintering began at 1150°C. However, the sintering process affected more composite prepared by coprecipitation method in comparison to the other two investigated samples. Close inspection of the EDS layered image obtained for composite synthesized by thermal decomposition revealed that the ferrite/barioferrite is mostly localized, although its amount is lower in comparison to other two samples. The localization also took the place in the case of sample prepared by microemulsion method. In the case of the sample prepared *via* coprecipitation, the highest degree of delocalization of ferrite/barioferrite phase was observed.
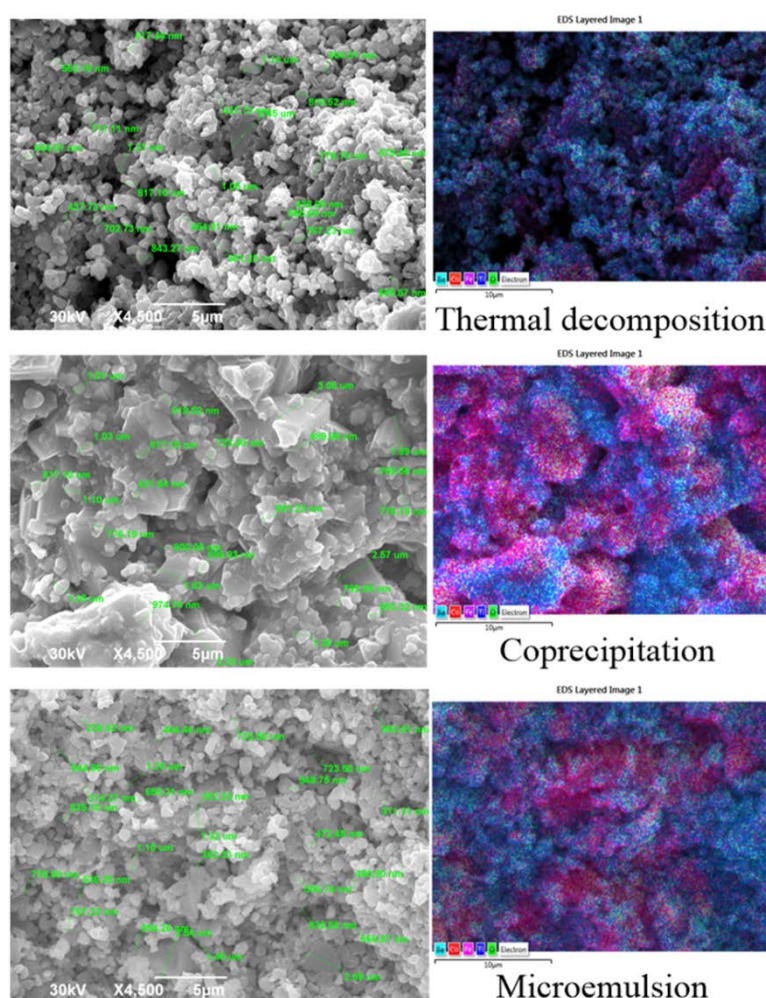

Fig. 3. SEM and EDS layered images of BaTiO$_3$/CoFe$_2$O$_4$ samples sintered at 1150°C.

SEM images obtained for the samples sintered at 1300°C showed that complete sintering has not occurred yet, although the high density regions were clearly seen, Fig. 4. However, the temperature dependent growth of the particles occurred, corroborating the sharpening reflexes and thus bigger crystallites in XRPD patterns. Sintering probably happened inside of formed agglomerates, causing porosity. For the material synthesized by coprecipitation method residues of liquid phase and the best ferrite/baroferrite delocalization were observed.
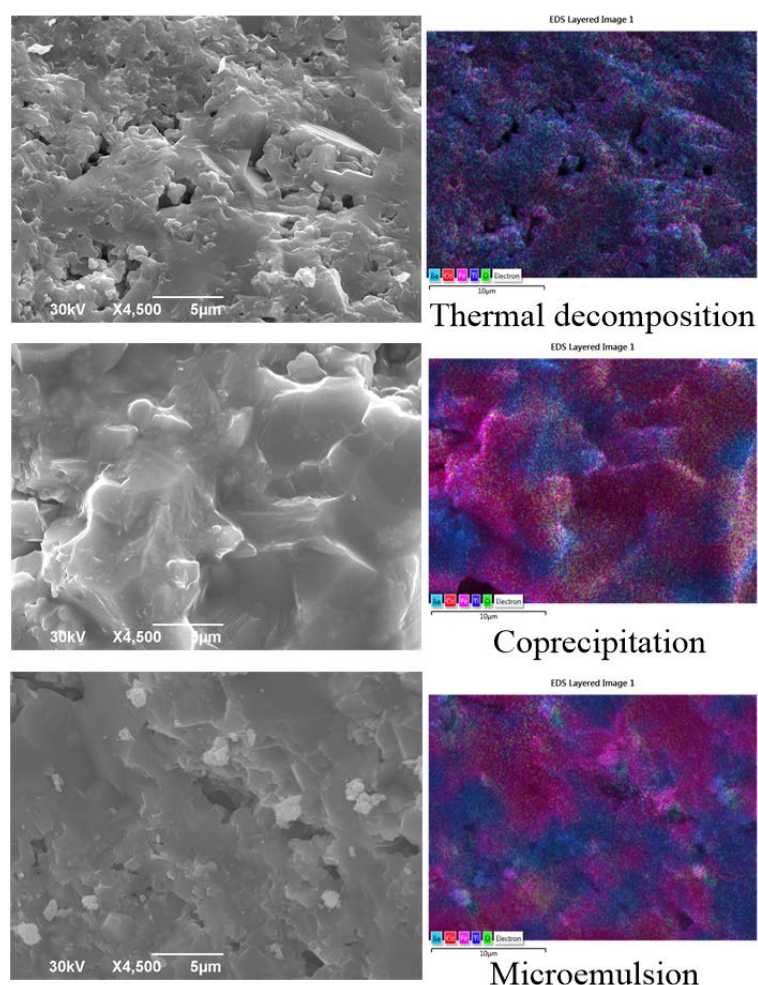
_____

Fig. 4. SEM and EDS layered images of BaTiO$_3$/CoFe$_2$O$_4$ samples sintered at 1300°C.

The relative dielectric constant and the loss tangent as a function of frequency measured at room temperature with corresponding Nyquist plots are presented in Fig. 5. Generally, the rise of dielectric constant with increasing sintering temperature was observed for all synthesized samples in the frequency range between 1kHz and 1 MHz [38,39]. In the case of samples sintered at 1300°C the curves presented in Fig. 5a followed the similar trend. In the low and mid frequency region the dielectric constant decreased with relatively small slope. On the other hand, in the high frequency region abrupt change of dielectric constant occurred, indicating strong frequency dependence. It is important to note that the sample obtained by microemulsion method sintered at 1300°C possessed order of magnitude bigger ε' value in comparison to other samples. This can be explained by the particle growth at temperature suitable to achieve dense ceramic bodies. Furthermore, the results of phase composition analyses indicated that the BaTiO$_3$ reacted with CoFe$_2$O$_4$ phase and formed hybrid barioferrite like phase which content is the highest for microemulsion synthesized sample sintered at 1300°C (≈26 %). Also, the amount of centrosymmetric SG *P4/mmm* BaTiO$_3$ phase, responsible for the cancelation of the dipole moments causing the zero net polarization in the material is the lowest (≈18%). In the case of sample prepared by thermal decomposition and sintered at 1300 °C, where the dielectric constant value was the smallest in comparison to other two samples, the amount of dominant centrosymmetric SG *P4/mmm* BaTiO$_3$ phase is ≈49%. However, the slope change of dielectric constant was the smallest indicating high stability in the wide frequency range. The loss tangents, presented in Figure

_____

5b, are lower compared to samples sintered at 1150°C in the low and mid frequency range showing that the temperature of 1300°C was high enough to achieve a sufficient sintering yielding dense ceramics. In other words, vacancies were kept at a minimum. In the high frequency range increased electric conductivity occurred as a consequence of direct conducting paths formation of grains. To gain a better understanding of the contribution of grain and grain boundaries to the dielectric response, the Nyquist plots were given, Fig. 5c.
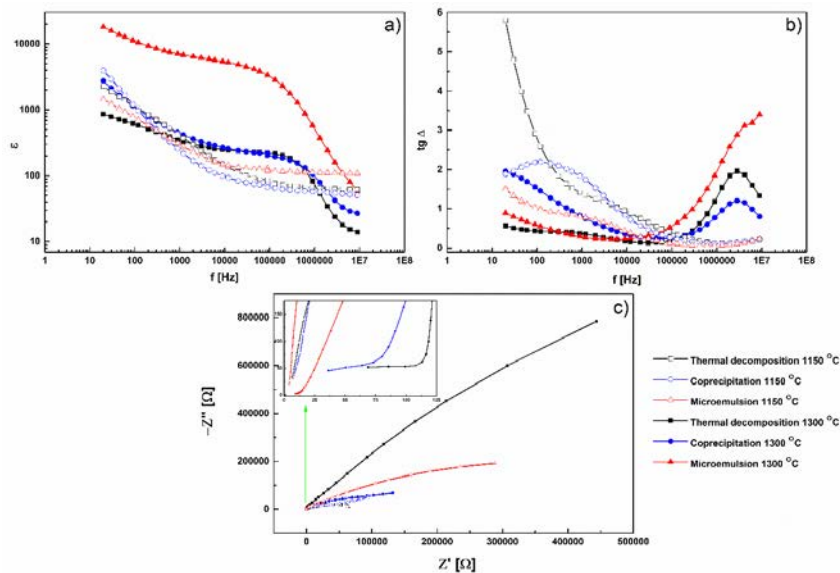
Fig. 5. a) Relative dielectric constant and b) tangent loss as a function of frequency with c) corresponding Nyquist plots for $BaTiO_3/CoFe_2O_4$ samples.

Tab. II Calculated grain and grain boundary resistivities and pseudo-capacities for all investigated samples.

Samples	R_g [Ω]	R_{gb} [Ω]	C_g [F]	C_{gb} [F]
$BaTiO_3/CoFe_2O_4$ thermal decomposition 1150 °C	5000	71947	3.22e-09	1.11e-08
$BaTiO_3/CoFe_2O_4$ coprecipitation 1150 °C	35157	396860	2.01e-09	3.50e-07
$BaTiO_3/CoFe_2O_4$ microemulsion 1150 °C	9858.1	730090	1.23e-08	1.93e-08
$BaTiO_3/CoFe_2O_4$ thermal decomposition 1300 °C	114.17	91085	1.07e-10	2.46e-09
$BaTiO_3/CoFe_2O_4$ coprecipitation 1300 °C	61.79	73592	2.56e-10	3.96e-09
$BaTiO_3/CoFe_2O_4$ microemulsion 1300 °C	20.39	11713	1.09e-09	1.18e-07

_____

Samples sintered at 1150°C, irrespective of synthesis procedure used, possessed some resistivity but also capacity that occurred due to the many isolated grains with undesired vacancies, in high frequency region. In the low and mid frequency range the only difference occurred in the case of microemulsion prepared sample where the amount of barioferrite like phase is the lowest (see Table I). Additional calcination at 1300°C led to better conductivity as a result of enhanced direct conducting paths formations. The eisanalyser software and equivalent circuit consisted of two parallel R-CPE elements connected in series were used to investigate the grain and grain boundary (GB) resistivity and pseudo-capacity, Table II. In the case of all samples grain boundary contribution is dominant [40, 41]. The values of grain and grain boundary resistivity and pseudo-capacity decreased with higher sintering temperature, irrespective of the synthesis used. The highest Rg value (114.17 Ω) was obtained for sample prepared by thermal decomposition method, while the lowest (20.39 Ω) was gained for the sample prepared in microemulsion manner. Grain boundary resistances and of samples sintered at 1300°C are noticeably lower than samples sintered at 1150°C while pseudo – capacities are order of a magnitude lower. Effective surface of GB interface is much lower due to better sintering of samples which is in direct correlation with GB capacity. Also, distances between grains are lower which gives higher probability of electron hoping trough GB region resulting in lower resistance. Previously mentioned is supported by SEM images of the samples.

An Arrhenius expression was used to additionally describe the dielectric relaxation process:

$$f = f_0 e^{-\left(\frac{E_a}{RT}\right)} \quad (1)$$

f_0 is the pre-exponential factor, E_a is the activation energy for the relaxation process, and R is the universal gas constant. The Arrhenius plots (ln f vs. 1000/T) shown in Fig. 6 exhibited a linear relationship.
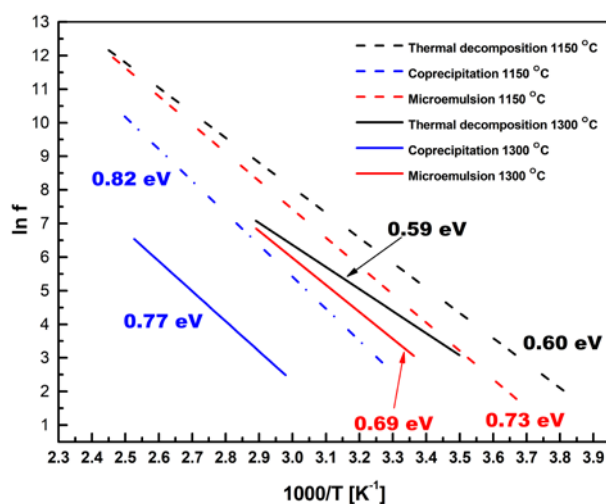

Fig. 6. Arrhenius relations of ln f versus 1000/T for the relaxation process for sintered BaTiO$_3$/CoFe$_2$O$_4$ samples.

In measured temperature/frequency range grain boundary relaxations contribution was recorded. Activation energies for the dielectric relaxation processes were: 0.60 eV, 0.82 eV, 0.73 eV for samples sintered at 1150°C and 0.59 eV, 0.77 eV, 0.69 eV for samples sintered at 1300°C. Obtained activation energies for these samples corresponds to reported BaTiO$_3$ values [42, 43]. Activation energies for the relaxation process indicated that the

_____

electrostatic potential barrier is a bit lower at GB for samples obtained at 1300°C. Activation energy depends on the sintering temperature applied [44], as well as on the grain size [45, 46]. As previously shown on SEM micrographs high density regions were clearly observed for sample sintered at 1300°C which led to lower values of E_a. This also corroborates previous analysis of Nyquist plots where modeled resistances (R_{GB}) of samples sintered at 1150°C show greater values than samples sintered at 1300°C, except for the sample obtained by thermal decomposition method where similar values of R_{GB} for both temperatures were observed.
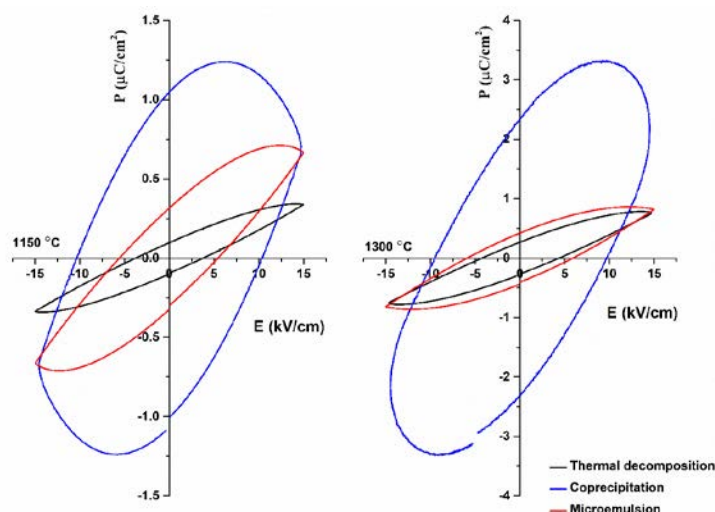

Fig. 7. Electrical hysteresis loops for sintered $BaTiO_3/CoFe_2O_4$ samples.

Hysteresis P-E loops for samples sintered at 1150°C and 1300°C measured at fixed frequency of 100 Hz were presented in Fig. 7. These ferroelectric loops were obtained by applying the electrical field in the range of 5–40 kV/cm for investigated ceramic samples. For the comparison purposes a field of 15 kV/cm was chosen. Ferroelectric measurements did not demonstrate well defined hysteresis loops, i.e. the saturation was not achieved due to low value of electric field (15 kV/cm). Moreover, the presence of cobalt ferrite phase, as a very conductive phase, as well as, interfacial polarization also contributed to the hysteresis loops shapes. It is very hard to talk about remnant or saturation polarization and coercive field because of presence of not well saturated ferroelectric loops [47], especially in the case of the samples prepared by coprecipitation. However, in the case where the sample was synthesised by thermal decomposition, the hysteresis was most similar to conventional hysteresis loop of ferroelectric materials. With the increase of barium-titanate phase (see Table I), coercive field at 15 kV/cm decreased in all cases. The leakage current was quite large for the sample obtained by coprecipitation method. This corresponds to the highest amount of the conductive ferrite and barioferrite phases obtained by XRPD. It is interesting to mention that the increase in sintering temperature mostly affected sample synthesized in microemulsion manner, reducing the current leakage significantly (Fig. 7). The increase in sintering temperature did not influence the loop obtained for the samples prepared by thermal decomposition and coprecipitation.

To reveal conductivity mechanism in the synthesized $BaTiO_3/CoFe_2O_4$ samples, the leakage current density (j) was presented as a function of static electric-field (E) presented on semi-logaritmic, Fig. 8, and logarithmic plots, Fig. 9. Sample synthesized by coprecipitation method showed the highest value for current leakage at both sintering temperatures which is in accordance with hystereses shapes. The logarithmic plots showed two distinct slope regions. There are four possible mechanisms of the conduction in these materials: grain

_____

boundary limited conduction (GBLC), ohmic conduction mechanism, space charge limited conduction (SCLC) or trap-controlled SCLC mechanism. In the low field region slope values were between 1.19 and 1.49 for all samples. This can be associated with Ohmic conduction mechanism where the thermally generated free carriers density is higher than the density of injected charge carriers. The slope values in the 1.58–4.94 range in the high field region suggested the existence of space-charge-limited-conduction (SCLC). In this region with SCLC the injected charge carriers dominate the conduction.
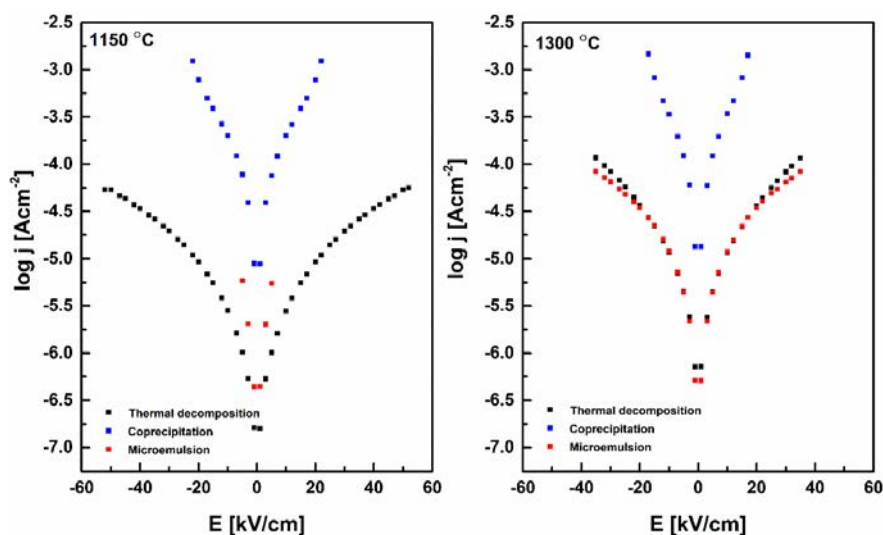

Fig. 8. Leakage measurements for $BaTiO_3/CoFe_2O_4$ samples as log j – E dependence.

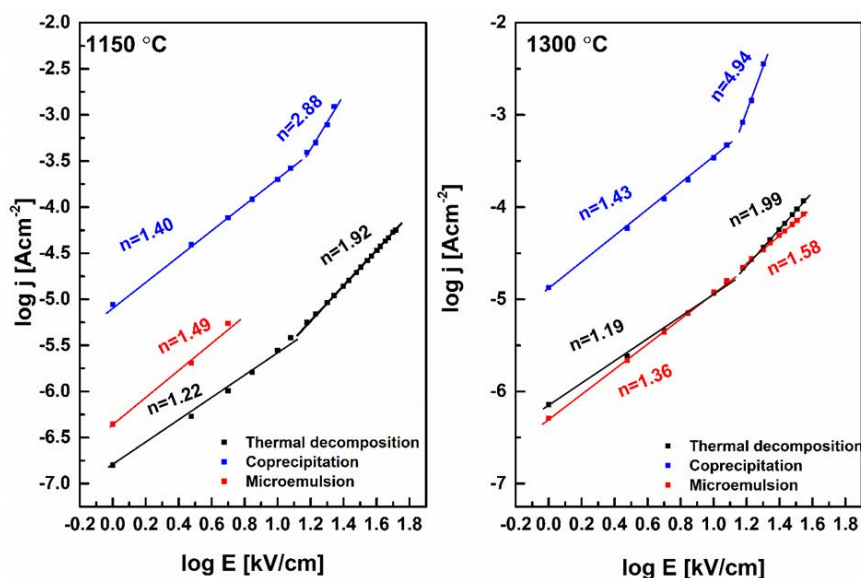**Fig. 9.** Leakage measurements for $BaTiO_3/CoFe_2O_4$ samples as log j – log E dependence.

4. Conclusion

The diphase $BaTiO_3/CoFe_2O_4$ composites were successfully synthesized using thermal decomposition, coprecipitation, and microemulsion method, and sintered at 1150°C

_____

and 1300°C. The phase composition and morphology were fully examined by XRPD and SEM/EDS analyses. The results of ferroelectric and dielectric measurements revealed better performances of the samples sintered at 1300°C than those calcined at lower temperature. The composite prepared in thermal decomposition manner showed high stability in the wide frequency range and low leakage currents due the lowest amount of the conductive ferrite phase responsible for deterioration of magnetoelectric response. The obtained results gave us a hope that such composite could be successfully used as a functional multiferroic.

Acknowledgments

5. References

1. M.A. Nazir, M. Ul-Islam, I. Ali, H. Ali, B. Ahmad, S.M. Ramay, N. Raza, M.F. Ehsan, M.N. Ashiq, Structural, J. Electron. Mater. 45 (2016) 1065.
2. Z. Manzoor, A. Khalid, G.M. Mustafa, S.M. Ramay, S. Naseem, S. Atiq, J. Magn. Magn. Mater. 500 (2020) 166409.
3. A.M. Moustafa, S.A. Gad, G.M. Turky, L.M. Salah, Structural, J. Solid State Sci. Technol. 11 (2022) 33008.
4. Y. Tokunaga, N. Furukawa, H. Sakai, Y. Taguchi, T. Arima, Y. Tokura, Nat. Mater. 8 (2009) 558.
5. R. Liu, Y. Zhao, R. Huang, Y. Zhao, H. Zhou, J. Mater. Chem. 20 (2010) 10665.
6. P. Augustine, Y. Narayana, N. Kalarikkal, Nanoscale Adv. 3 (2021) 4866.
7. J.S. Bangruwa, B.K. Vashisth, N. Singh, N. Singh, V. Verma, J. Alloys Compd. 739 (2018) 319.
8. V. Buscaglia, C.A. Randall, J. Eur. Ceram. Soc. 40 (2020) 3744.
9. V. Paunović, Z. Prijić, V. V. Mitić, Sci. Sinter. 54 (2022) 81.
10. S. Filipović, L. Anđelković, D. Jeremić, P. Vulić, A.S. Nikolić, S. Marković, V. Paunović, S. Lević, V.B. Pavlović, Sci. Sinter. 52 (2020) 257.
11. T. Tsurumi, T. Hoshina, H. Takeda, Y. Mizuno, H. Chazono, IEEE Trans. Ultrason. Ferroelectr. Freq. Control. 56 (2009) 1513. doi:10.1109/TUFFC.2009.1214.
12. W.P. Mason, R.F. Wick, J. Acoust. Soc. Am. 23 (1951) 209.
13. P. Tang, D.J. Towner, A.L. Meier, B.W. Wessels, Appl. Phys. Lett. 85 (2004) 4615.
14. M. Wegmann, R. Brönnimann, F. Clemens, T. Graule, Sensors Actuators A Phys. 135 (2007) 394.
15. D.S. Mathew, R.-S. Juang, Chem. Eng. J. 129 (2007) 51.
16. C.O. Ehi-Eromosele, I.B. Iserom, I.E.E. Joshua, Sci. Sinter. 48 (2016) 221.
17. S.B. Narang, K. Pubby, J. Magn. Magn. Mater. 519 (2021) 167163.
18. H. Wu, G. Liu, X. Wang, J. Zhang, Y. Chen, J. Shi, H. Yang, H. Hu, S. Yang, Acta Biomater. 7 (2011) 3496.
19. G. Wang, Y. Ma, Z. Wei, M. Qi, Chem. Eng. J. 289 (2016) 150.
20. M. Pardavi-Horvath, J. Magn. Magn. Mater. 215–216 (2000) 171.
21. E. Schloemann, J. Magn. Magn. Mater. 209 (2000) 15.
22. T. Tatarchuk, M. Bououdina, J. Judith Vijaya, L. John Kennedy, Spinel Ferrite Nanoparticles: Synthesis, Crystal Structure, Properties, and Perspective Applications, in: O. Fesenko, L. Yatsenko (Eds.), Nanophysics, Nanomater. Interface Stud. Appl.,

Springer International Publishing, Cham, 2017: pp. 305–325.

23. B.I. Kharisov, H.V.R. Dias, O. V Kharissova, Arab. J. Chem. 12 (2019) 1234.
24. K.C. Verma, M. Singh, R.K. Kotnala, N. Goyal, J. Magn. Magn. Mater. 469 (2019) 483.
25. M. Vinyas, S.C. Kattimani, Compos. Struct. 185 (2018) 51.
26. H. Yang, G. Zhang, Y. Lin, J. Alloys Compd. 644 (2015) 390.
27. M. ud Din Rather, R. Samad, N. Hassan, B. Want, J. Alloys Compd. 794 (2019) 402–416.
28. M. Etier, V. V Shvartsman, S. Salamon, Y. Gao, H. Wende, D.C. Lupascu, J. Am. Ceram. Soc. 99 (2016) 3623.
29. D. Erdem, N.S. Bingham, F.J. Heiligtag, N. Pilet, P. Warnicke, C.A.F. Vaz, Y. Shi, M. Buzzi, J.L.M. Rupp, L.J. Heyderman, M. Niederberger, ACS Nano. 10 (2016) 9840.
30. A. Ruiz, M. Nair, A. Kaushik, Sci Lett J. 4 (2015) 172.
31. S. Mhambi, D. Fisher, M.B. Tchoula Tchokonte, A. Dube, Pharmaceutics. 13 (2021) 1479.
32. R. Guduru, P. Liang, J. Hong, A. Rodzinski, A. Hadjikhani, J. Horstmyer, E. Levister, S. Khizroev, Nanomedicine. 10 (2015) 2051.
33. B.N. Rao, P. Kaviraj, S.R. Vaibavi, A. Kumar, S.K. Bajpai, A. Arockiarajan, J. Appl. Phys. 122 (2017) 164102.
34. D. Dominguez-Paredes, A. Jahanshahi, K.L. Kozielski, Brain Stimul. 14 (2021) 1285.
35. S. Kopyl, R. Surmenev, M. Surmeneva, Y. Fetisov, A. Kholkin, Mater. Today Bio. 12 (2021) 100149.
36. L. V Leonel, J.B. Silva, A.S. Albuquerque, J.D. Ardisson, W.A.A. Macedo, N.D.S. Mohallem, J. Phys. Chem. Solids. 73 (2012) 1362.
37. L.M. Hrib, O.F. Caltun, J. Alloys Compd. 509 (2011) 6644.
38. X. Zhang, G. Chen, C. Fu, W. Cai, R. Gao, F. Wang, Process. Appl. Ceram. 12 (2018) 45.
39. Q.H. Jiang, Z.J. Shen, J.P. Zhou, Z. Shi, C.-W. Nan, J. Eur. Ceram. Soc. 27 (2007) 279.
40. L. Weng, Y. Fu, S. Song, J. Tang, J. Li, Scr. Mater. 56 (2007) 465.
41. R.P. Mahajan, K.K. Patankar, M.B. Kothale, S.C. Chaudhari, V.L. Mathe, S.A. Patil, Pramana - J. Phys. 58 (2002) 1115.
42. V.H. Schmidt, N. Archer, C.-S. Tu, J. Am. Ceram. Soc. 101 (2018) 713.
43. Y. Leyet, F. Guerrero, J.P. de la Cruz, Mater. Sci. Eng. B. 171 (2010) 127.
44. S. Breuer, D. Prutsch, Q. Ma, V. Epp, F. Preishuber-Pflügl, F. Tietz, M. Wilkening, J. Mater. Chem. A. 3 (2015) 21343.
45. M.V.F. Heinz, M.-C. Bay, U.F. Vogt, C. Battaglia, Acta Mater. 213 (2021) 116940.
46. L. McGovern, I. Koschany, G. Grimaldi, L.A. Muscarella, B. Ehrler, J. Phys. Chem. Lett. 12 (2021) 2423.
47. A.S. Dzunuzovic, M.M.V. Petrovic, J.D. Bobic, N.I. Ilic, B.D. Stojanovic, J. Electroceramics. 46 (2021) 57.

Сажетак: *У циљу испитивања утицаја методе синтезе као и температуре синтеровања на функционална својства керамике перовскитно/спинелне структуре, синтетисани су $BaTiO_3/CoFe_2O_4$ композити методама термалне декомпозиције, копреципитације и микроемулзије, а затим синтеровани на 1150 °C и 1300 °C. Фазни састав и морфологија синтетисаних узорака детаљно су испитани пре и после синтеровања помоћу рендгенске дифракције на праху (XRPD) и скенирајуће електронске микроскпије (SEM) спрегнуте са елекрон дисперзивном спектроскопијом (EDS). Изведена су опсежна испитивања како диелектричних, тако и*

_____

фероелектричних својстава датих композита. У већини случајева узорци синтеровани на 1300 °C показали су боља својства од узорака синтерованих на 1150 °C. Композит синтетисан методом термалне декомпозиције и синтерован на 1300 °C издваја се од осталих синтетисаних BaTiO₃/CoFe₂O₄ узорака захваљујући великој стабилносту у широком фреквентном опсегу и малим струјама цурења. Добијени резултати недвосмислено указују да истакнути композит може бити успешно примењен као функционални мултифероик.

Кључне речи*: Перовскитно/спинелна керамика; Мултифероици; Синтеровање; Утицај методе синтезе.*